

Effect of submarine canyons on tsunami heights, currents and run-up off the southeast coast of India

Jaya Kumar Seelam^{1,*}, R. Mani Murali¹ and T. E. Baldock²

¹National Institute of Oceanography, Goa 403 004, India

²University of Queensland, School of Engineering, St. Lucia, QLD 4072, Australia

Tsunami numerical model studies are mostly focused on inundation and run-up onto the coast. Fewer studies have been aimed at investigating the role of submarine canyons on tsunami heights, currents and run-up. The tsunami hydrodynamics in the vicinity of submarine canyons and ridges in the Palar–Cauvery region off the southeast coast of India on 26 December 2004 is considered in this study. Numerical modelling was carried out to study tsunami heights and currents in the vicinity of the submarine canyons as well as the variation of tsunami heights at 10 m water depth. Comparisons between the tsunami wave energy density at 10 m depth and the onshore run-up height observations showed good correlation for select locations, with the run-up heights being about 3% of the wave energy density. However, the local topography in the run-up zone also strongly influences the local run-up, which reduces direct correlations between run-up and nearshore tsunami height.

Keywords. Flow velocity, numerical modelling, run-up height, submarine canyons, tsunami.

THE effect of tsunamis on the coastal regions has been devastating in the recent years despite the technological advancements in tsunami detection and warning systems available around the world. The generation of a tsunami and its impact on the coast depend on many parameters, including source parameters, proximity to the coast, topography of the seabed, etc.^{1,2} Submarine canyons and ridges are one such topographic feature of the seabed that could affect tsunami propagation. As submarine canyons have steep slopes, they are prone to slope failure leading to submarine landslides (slumping) and thus the generation of turbidity currents. The submarine canyon system slope stability is related to the processes modifying the slopes and external triggering mechanisms that cause them to fail. Large sediment mass or debris flowing through these canyons or strong turbidity currents would pose problems for any subsea installation³.

Most of the Indian Ocean tsunami-related studies^{4–6} are focused on source parameters, travel time and time of arrival^{7–12}, coastal inundation or run-up height measurements and modelling. Although a few studies along the Indian coast hint at the amplification of the tsunami and therefore increase in run-up heights¹³, not many studies are available on the tsunami-induced currents in the vicinity of submarine canyons. Moreover, the literature on the effect of canyons on these currents is not readily accessible. Not many detailed modelling studies exist on the modification of the December 2004 tsunami due to submarine canyons on the east coast of India, except for Divyalakshmi *et al.*¹⁴ and Seelam and Baldock¹⁵. However, observations suggest a significant impact from submarine bathymetry, leading to complex scattering and amplification of tsunami run-up due to canyons and coastal bays¹⁶. With regard to the Indian Ocean basin, some of the major differences between the present study and that of Divyalakshmi *et al.*¹⁴ are: (i) the initial source driving the tsunami is realistic and based on verified literature and includes both positive and negative elevation of the initial tsunami source, whereas a single hump of positive surface elevation was considered by Divyalakshmi *et al.*¹⁴; (ii) The method of analysing the tsunami variations is different: discrete points were studied by Divyalakshmi *et al.*¹⁴, whereas spatial variation along a canyon and a ridge are studied here; (iii) Divyalakshmi *et al.*¹⁴ studied only the change in tsunami height from a single hump source, whereas the present study includes velocity components along the canyon and ridge lines using a much more reasonable tsunami source. Seelam and Baldock¹⁵ used a preliminary tsunami initial source model of USGS in a 3D hydrodynamic model and estimated the bed shear stresses using the near-bottom flow velocities. The source model used did not provide realistic comparison with the tsunami height observations and therefore is not further discussed here.

Previous literature focusing on other geographical areas or on the general behaviour of tsunami propagation has studied the effect of submarine canyons and ridges in an idealized scenario. A considerable difference occurs in the tsunami behaviour depending on the distance between the canyon and the shoreline, or if the canyon extends to

*For correspondence. (e-mail: jay@nio.org)

the shore. Numerical modelling by Roger and Hébert¹⁷ indicated the modification of nearshore wave heights by submarine canyons, but no observation data were available for verification. Other notable studies are those by Aránguiz and Shibayama¹⁸, and Iglesias *et al.*¹⁹. Using idealized bathymetry, and no ridges formed by adjacent canyons, these studies showed a reduced run-up behind the canyon and an increase in run-up and tsunami amplification at the adjacent coasts, which were consistent with field observations. The results are sensitive to canyon width, length and depth, and are thus site-specific. In addition, the general conclusions apply to an idealized shore normal canyon which does not extend to the shore. Ioualalen *et al.*²⁰ have noted the protective influence of canyons in the Indian Ocean, which sheltered Bangladesh from the major impacts of the 2004 Indian Ocean tsunami, although some localities experienced significant tsunami amplification. Related work has considered the influence of shoreline shape (bay shape) on nearshore tsunami magnification²¹, or both a nearshore canyon and associated narrow bay^{22,23}. In each case, amplification of the run-up is much greater than that which occurs for a plane longshore uniform beach. However, for offshore canyons the effect of the bathymetry can be different, since refraction can occur in this case.

Thus, while general principles identified by Aránguiz and Shibayama¹⁸, and Iglesias *et al.*¹⁹ indicate the overall effect of canyons, care is needed when applying those findings to more complex natural bathymetry, and high-quality field data are also needed for Model verification. The effect of the canyons and ridges present on the southeast coast of India on the local tsunami run-up heights has not been modelled in previous studies, nor have there been model comparisons with local field data along this coast. This article showcases the changes in flow pattern and tsunami magnitude around submarine canyon and ridge system found on the southeast coast of India, and their influence on the run-up height on the coast, which have not been reported thus far at these locations.

Study area

The southeast coast of India has been one of the worst affected regions during December 2004 tsunami event (Figure 1). The present study region comprises the most affected area on the mainland Indian subcontinent. The study region on the southeast coast of India, including the state of Tamil Nadu and Union Territory of Puducherry, comprises a number of interesting landforms, including mudflats, sandy beaches, mangroves, marshy regions, river deltas, creeks, beach ridges, etc.²⁴. The hinterland along this coast is extremely flat and the foreshore regions comprise narrow, low beaches in the southern

region to high dune system in the northern region. The topography of the continental shelf off the east coast of India is relatively uniform, except for some canyons cutting deeply into the shelf²⁵.

Submarine canyons off Madras coast were identified in the 15th cruise of INS *Kistna* during 1964 (ref. 26). Varadachari *et al.*²⁵ analysed earliest data on the submarine canyons based on bathymetric surveys conducted during the 26th cruise of INS *Kistna* and their bathymetry analysis showed the existence of three sets of distinctly different canyons cutting across the shelf and slope regions near Cuddalore (11°45'N; 79°47'E) and Puducherry (11°54'N; 79°52'E). The southernmost canyon is named as Cuddalore Canyon, the northern most as Palar Canyon and the middle one as Pondicherry Canyon (Figure 2). The influence of Pondicherry Canyon on the tsunami has been considered in this study, and any references to the canyon in general would indicate the Puducherry Canyon. The effect of these canyons and ridges on the local tsunami run-up heights and currents has not been modelled in previous studies. Therefore, in order to assess the effect of the Pondicherry canyon, two transects, one along the centre line of the canyon (marked as C1–C2 in Figure 2) and the other along the ridge (marked as R1–R2 in Figure 2), were considered. Figure 3 shows a cross-section along the centre line of this canyon as well as across the ridge to the south of this canyon. The bottom slope of the canyon is steeper (~1 : 6.25) compared to that of the ridge (~1 : 32). It is also observed that along the ridge the continental shelf is wider by 10 km compared to that along the canyon.

Post-tsunami survey

A number of post-tsunami surveys were carried out along the tsunami hit region in the southeast coast of India^{4,27–34}, mostly using the UNESCO guidelines³⁵. A detailed report is available on a tsunami survivor's eyewitness records, beach and hinterland profiles from water line to the maximum inundation limits at select locations, run-up heights, tsunami levels along the buildings, etc.³⁶. The run-up heights were estimated at various locations from the maximum inundation limits and the mean sea level⁴. Many of the tide gauges along the coast of India as well as in the Indian Ocean recorded tsunami arrival times and analysis of these tidal elevations provided the tsunami heights along the coast. The maximum run-up height measured along the southeast coast of India was of the order of 6.2 m asl. The run-up heights were observed to increase abnormally at certain locations compared to adjacent locations, e.g. with reference to the station located along 12°N lat. (ref. 4) the maximum run-up height was about 6.2 m whereas it was about 4 m within a distance of about 30 km on both sides. This sudden variation in run-up heights within a short distance was not addressed in

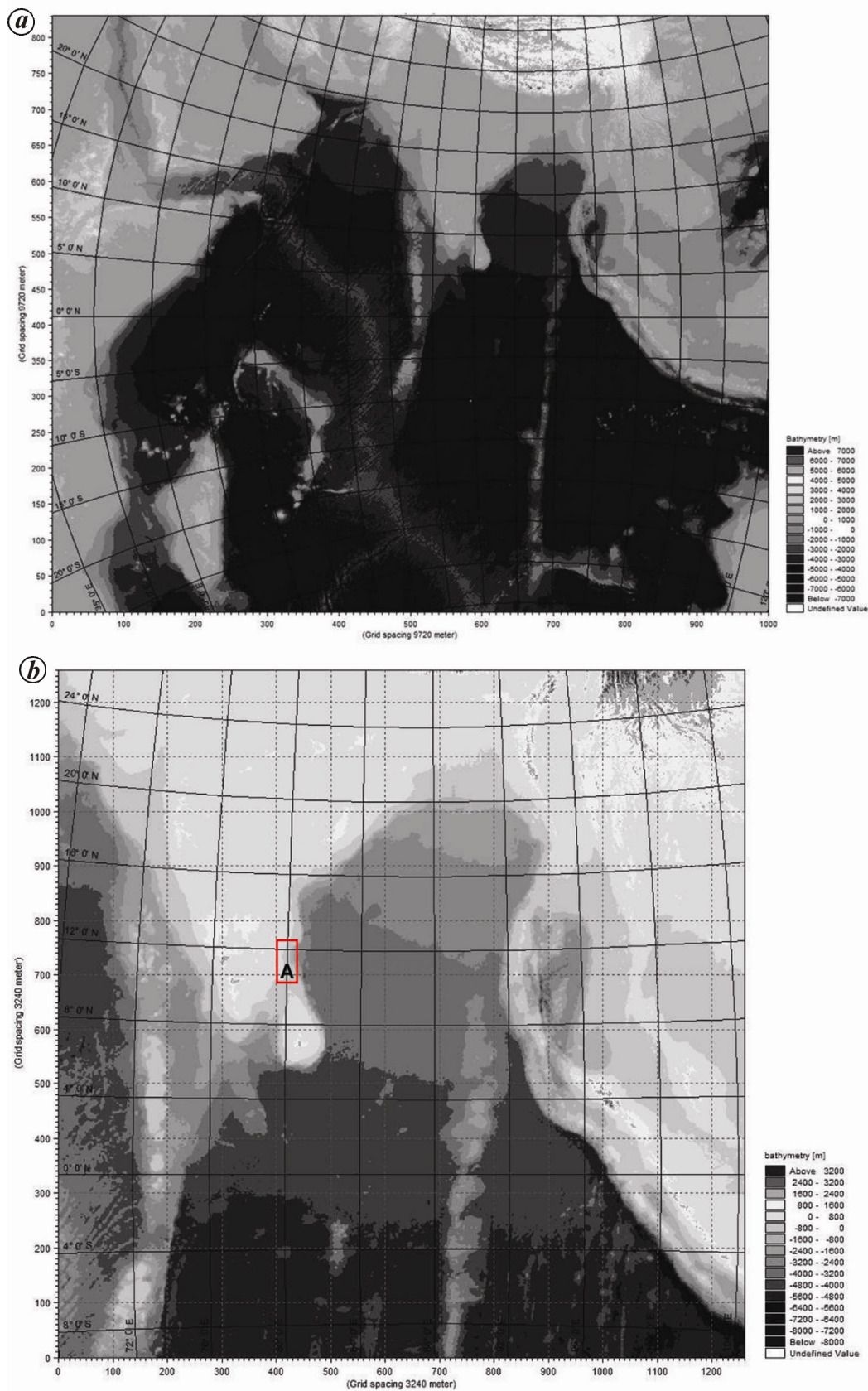


Figure 1. *a*, Global model domain covering the Indian Ocean. *b*, Regional model domain used for tsunami propagation including the Bay of Bengal and eastern Arabian Sea. Area marked as 'A' inside the rectangle is local model domain shown in Figure 2.

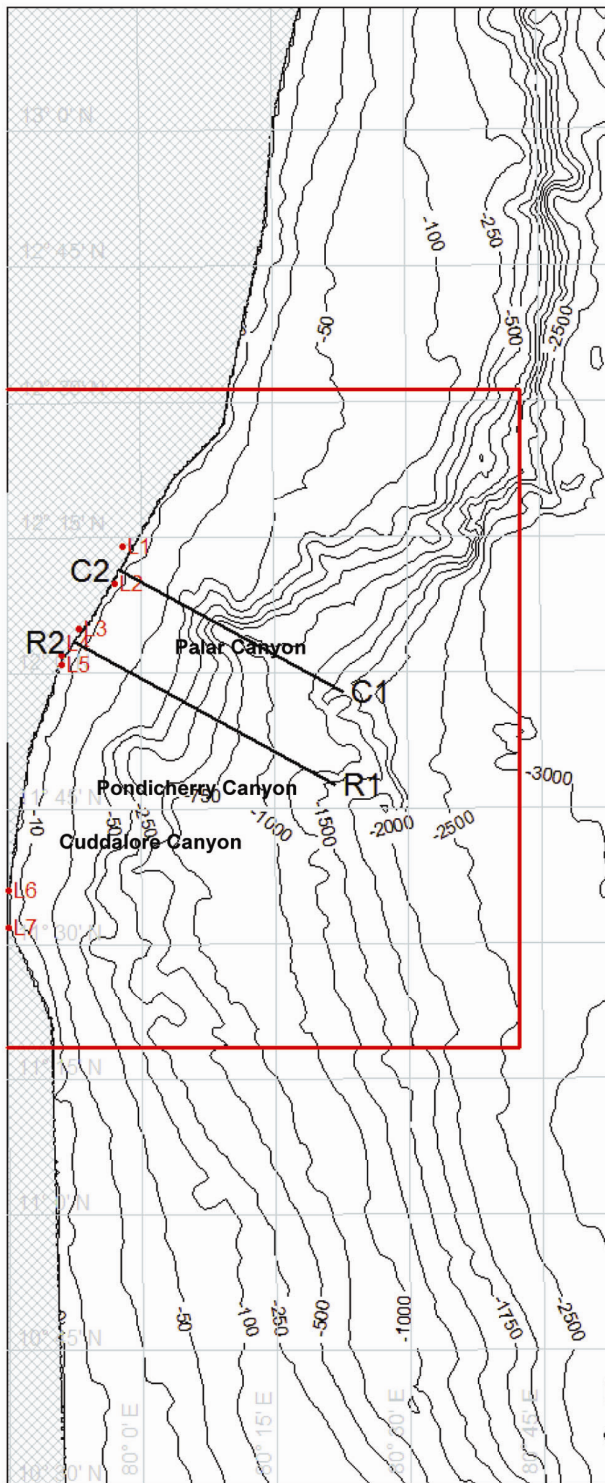


Figure 2. Local model domain used for tsunami propagation. Thin lines are isobaths. The region considered for the study is enclosed in rectangle. C1–C2 and R1–R2 are profiles along the canyon and ridge. L1–L7 are locations mentioned in Table 2.

earlier studies^{4,5,27,37}. In this article, the increase in run-up height which is related to increased tsunami height is addressed in terms of the impact caused by the submarine canyon present in the vicinity.

Methodology

Tsunami propagation simulations were carried out for the above study region using MIKE21 (ref. 38), a depth-averaged hydrodynamic model that has been verified to provide reliable comparisons with the measurements. The flow field in the hydrodynamic model is calculated by solving depth-integrated continuity and momentum equations. Alternating Direction Implicit technique is used to integrate the mass and momentum equations. A double-sweep algorithm is used to resolve the equation matrices that result for each direction and each individual grid line. Vertically integrated equations of conservation of volume and momentum in the x and y directions are used in the model. Coriolis terms, eddy viscosity using Smagorinsky formulation and bed friction are also included in the model³⁸. Figure 4 shows the model domains adopted in the study. The global model domain used has 9.72 km square grid, comprising the coastlines surrounding India, Sri Lanka, Africa, Indonesia, Australia, etc.

The regional model with 3.24 km square grid, comprising the Bay of Bengal, India, Sri Lanka towards west of the tsunami source, is considered with the bathymetry obtained from ETOPO2 data. The tsunami sources were used in a nested tsunami propagation model with the outer model covering a region comprising the Indian Ocean (Figure 1 *a*) and a regional model (Figure 1 *b*) covering the Bay of Bengal. In order to resolve the nearshore bathymetry, including the canyons and ridges, as well as to represent the adjoining coastline appropriately, a local model with a finer grid size of 300 m taken from the hydrographic charts of the region was considered (Figure 2). Tsunami propagation over the regional model domain was carried out for 6 h and the results were compared with the arrival times and the first wave magnitudes at six different locations. Tides, winds and waves were not included in the model since the intention of the study was to understand tsunami-induced heights and currents.

Tsunami initial surface elevation

The tsunami initial surface elevation or tsunami source is an important input to any tsunami propagation model. One of the preliminary seabed uplift maps for the December 2004 earthquake available soon after the event was from the United States Geological Survey (USGS) website, currently available at <http://earthobservatory.nasa.gov/NaturalHazards/view.php?id=14406>. The northern extent of the tsunami source region in this uplift map was below the 6°N lat. Whereas later studies indicated tsunami source extending till 9°N (ref. 39). Numerical simulations of tsunami propagation using the tsunami source map up to 6°N did not result in good comparison with the measurements in the north Indian Ocean region⁵. Using the tsunami source curtailed to 6°N, the derived

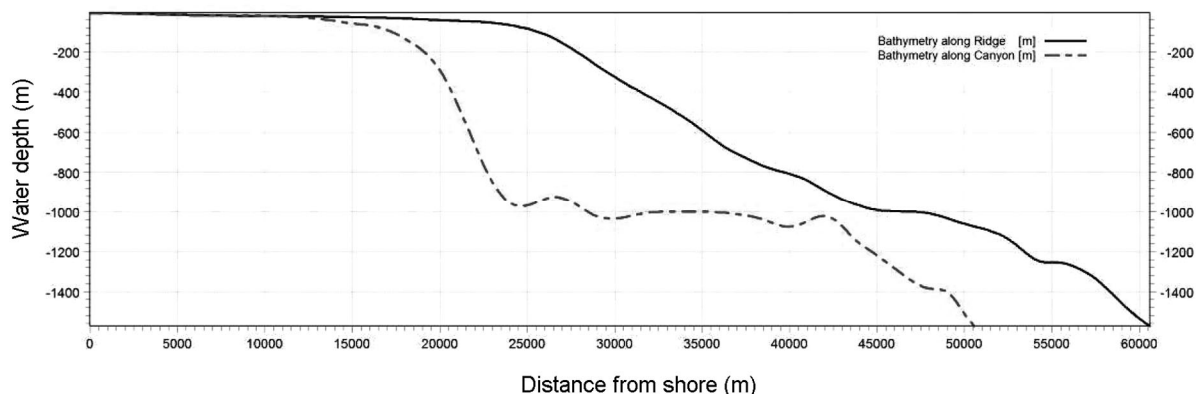


Figure 3. Profile along the canyon (C1–C2) and ridge (R1–R2) (see Figure 2 for location of ridge and canyon).

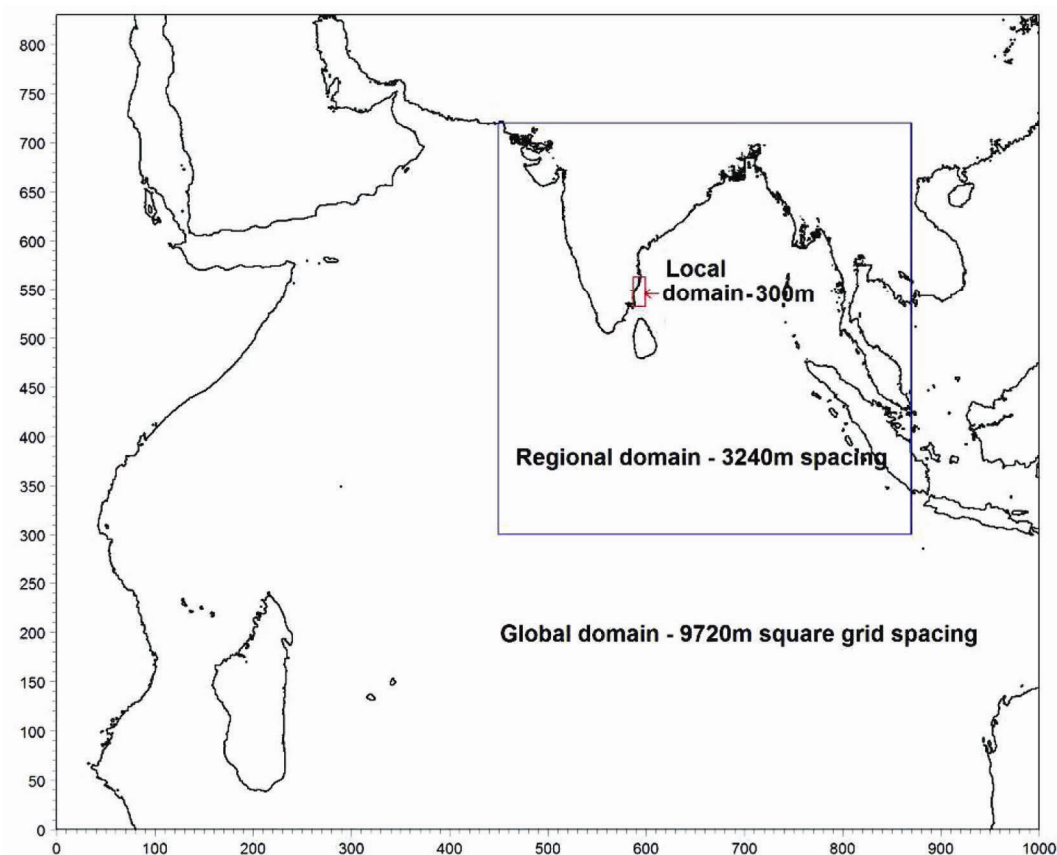


Figure 4. Model domains used in the study. Global domain covering the Indian Ocean is made of square grid spaced at 9720 m, regional domain covering the Bay of Bengal and eastern Arabian Sea is made of square grid spaced at 3240 m and local domain covering the southeast Tamil Nadu coast is made of square grid spaced at 300 m.

tsunami arrival times were within a few minutes difference from the measurements; the magnitudes did not match well. Studies on the extent of the tsunami source region resulted in a region that is much beyond 6°N (refs 2, 39–41). The initial sea surface displacement used by Titov *et al.*² extending almost till 15°N was derived based on the region of the earthquake; comparison of the model results with the Jason-1 satellite altimeter readings showed that the model provided the initial tsunami wave crest,

but not the trough and trailing part of the waves^{1,42}. Vigny *et al.*⁴³ derived the tsunami source based on GPS and uplift observations; their tsunami propagation simulations did not result in accurate tsunami arrival times compared to the measured tide gauge data. Song *et al.*⁴⁴ used a 3D Ocean General Circulation model in conjunction with the seismic form wave inversion and compared the model results with satellite-derived data. However, their model results could not capture the twin peaks of

Table 1. Comparison of tsunami arrival time and magnitude of tsunami first wave (FW) crest at different locations⁴⁹ for different initial water level conditions obtained from Pietrzak *et al.*⁴¹ (Model-3), Pedersen *et al.*⁴⁵ (Alfa) and Grilli *et al.*⁴⁰ (Grilli)

Station	Arrival time UTC (h : min)				FW magnitude (cm)			
	Measured	Model-3	Alfa	Grilli	Measured	Model-3	Alfa	Grilli
Paradip	3 : 30	4 : 00	3 : 40	3 : 47	89	44	86	84
Visakhapatnam	3 : 40	3 : 40	3 : 19	3 : 36	65	76	120	116
Chennai	3 : 35	3 : 24	3 : 30	3 : 30	64	187	230	138
Male	4 : 16	4 : 11	4 : 18	4 : 18	146	96	116	154
Tuticorin	4 : 23	4 : 08	4 : 20	4 : 17	100	64	78	106
Kochi	5 : 41	5 : 23	5 : 31	5 : 36	84	46	52	97

the initial wave as seen in Jason-1 altimeter data. Pietrzak *et al.*⁴¹ used both GPS data in co-seismic displacement models and a tsunami propagation model to obtain a better source description. However, their study did not culminate in any single source, as all their surface elevation models had discrepancies with the satellite-derived tsunami height or arrival times. Model-2, model-3 and model-5 of Pietrzak *et al.*⁴¹ did not provide good comparisons with satellite altimeter data for the tsunami surface elevation derived from Jason-1 satellite. Their model-4 provided comparable initial wave height magnitude, but the rest of the wave did not correspond to the satellite data. However, the model-3 tsunami source results showed double-peaked initial wave in their study. Pedersen *et al.*⁴⁵ used the ALPHA geological model (<http://www.ahec.jp/>) with three distinct uplift regions in MIKE21 to simulate the tsunami propagation. Their source model resulted in mimicking the initial tsunami height to a reasonable extent, but did not capture the trough and second peak accurately. Grilli *et al.*⁴⁰ used an initial surface elevation obtained based on the Okada⁴⁶ formulation considering five segments. Comparison of the tsunami heights obtained from a Boussinesq long-wave propagation model FUNWAVE⁴⁷ simulation resulted in overall trend of the tsunami heights along the Jason-1 satellite track data of tsunami heights. However, the tsunami height magnitudes were underestimated by their model.

Different researchers used different tsunami initial surface elevation in different numerical models and compared with the observed tsunami heights, mostly along Jason-1 satellite track. In this article we simulated three different tsunami initial surface elevation sources using a tsunami propagation numerical model so as to confirm the applicability of these initial sources for further study. The three initial surface models selected are: (i) model-3 constructed by Pietrzak *et al.*⁴¹; (ii) Alfa model used by Pedersen *et al.*⁴⁵ with modified fault lengths and (iii) the Okada⁴⁶ formulation considering five segments used by Grilli *et al.*⁴⁰ (Figure 5). The tsunami propagation model results were compared with measured tsunami wave heights and arrival times at various locations along the southeast coast of India and along the Jason-1 satellite

track, to further select the best tsunami initial surface elevation model to study the influence of submarine canyons and tsunami-induced currents.

Numerical modelling of tsunami propagation

Numerical modelling of tsunami propagation and hydrodynamics of the study region were carried out using the hydrodynamics (MIKE-HD) module Mike by DHI³⁸, a state-of-the-art numerical model for simulating coastal and ocean hydrodynamics. The MIKE-HD module calculates the flow field by solving depth-integrated continuity and momentum equations using the Alternating Direction Implicit technique to integrate the mass and momentum equations. The equation matrices that result for each direction and each individual grid line are resolved by a Double Sweep algorithm⁴⁸. Vertically integrated equations of conservation of volume and momentum in x and y directions were used in the model. Eddy viscosity and Coriolis terms were also included, but these were mostly used for calibrating the model. The Smagoransky formulation of the eddy viscosity was used with a constant value of 0.5 and a bed resistance in terms of Manning's roughness of 64 was used for the entire domain. The model simulations were carried out for a period of 6 h with a time-step interval of 15 s resulting in a maximum Courant number of 1.16. The MIKE-HD model has been forced with a static tsunami initial surface elevation at initial time-step. No other input forcing either from wind, wave, or tide to the model was used. The open-water boundaries were forced with constant elevation of 0 m and the land boundaries were reflective. The output parameters of surface elevation and depth averaged currents over the entire model domain were stored at every minute and used for further analysis.

Results

Comparison of model results with observations

The tsunami arrival times, and initial tsunami height derived from the three models were also compared with

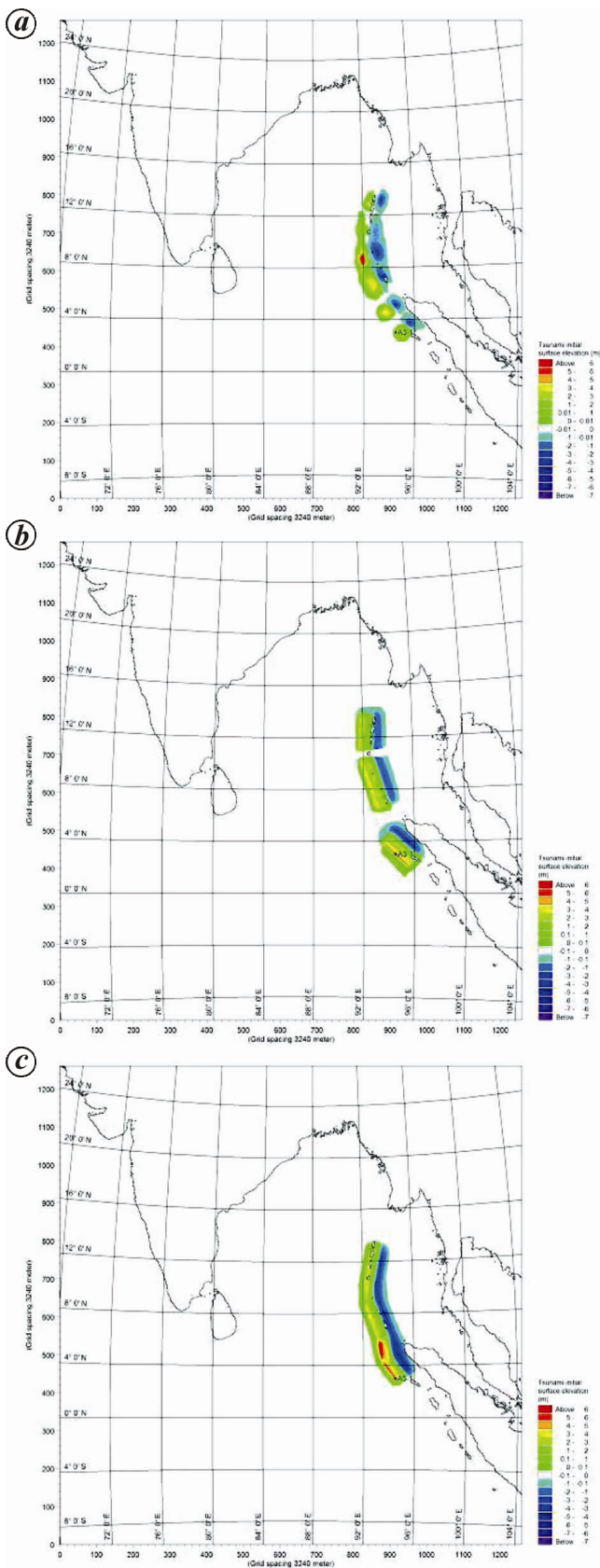


Figure 5. Tsunami source surface elevation from: (a) modified Model-3 of Pietrzak *et al.*¹⁹; (b) modified Alfa of DHI-Denmark⁴⁵ and (c) Grilli *et al.*⁴⁰.

the measurements available from the literature⁴⁹ (Table 1). The comparisons show that the model forced with Grilli *et al.*⁴⁰ tsunami source provides a better result compared to other tsunami source models considered here. The tsunami surface elevation along the Jason-1 satellite track, derived using the tsunami source models in Pietrzak *et al.*⁴¹, Pedersen *et al.*⁴⁵ and Grilli *et al.*⁴⁰ was compared with the satellite-derived tsunami height data (Figure 6). The Alfa model-derived tsunami height provides a higher initial wave and a larger trough than observed. The second peak is underestimated and so is the trailing wave train. Model-3-derived tsunami heights shows an increased second peak, but the initial peak was highly underestimated. However, the trough of the tsunami wave is represented well. The initial tsunami peak, trough and the second peak and the large trough as seen in the satellite data are reproduced well by the Grilli *et al.*⁴⁰ tsunami source models. The second peak is underestimated and the second trough in the trailing waves is highly underestimated. However, since only the first two waves are being considered in this study, the simulation results of Grilli *et al.*⁴⁰ tsunami source model which provide better representation of the measurements are further used in forcing the local domain, to study the hydrodynamics in the vicinity of the submarine canyons. The present study is limited to the tsunami heights and flow velocities generated by the initial waves. The secondary waves and currents generated by the later propagation of the tsunami, including its reflection from the coast are not examined.

Tsunami propagation and height

Snapshots of propagation of the tsunami front are studied at various time intervals representing important events, i.e. (i) tsunami initial wave crest reaching the foot of the canyon at 02 : 57 h; (ii) tsunami initial wave crest covered over the canyon at 03 : 25 h; (iii) maximum tsunami wave at landfall along canyon transect at 3 : 30 h; (iv) maximum tsunami wave at landfall along the ridge transect at 3 : 36 h; (v) tsunami second wave crest having landfall along canyon transect at 3 : 51 h; (vi) tsunami second wave crest having landfall along ridge transect at 3 : 58 h; (vii) maximum tsunami wave trough at coast along canyon transect at 4 : 20 h and (viii) maximum tsunami wave trough at coast along ridge transect at 4 : 28 h. Figure 7 is a spatial representation of the tsunami height contours for each of the eight events during the first two tsunami waves. The extent of crests and troughs and the spatial variation of the tsunami, refraction, diffraction and shoaling patterns of the tsunami waves spatially can be observed from the figure.

Figure 8 shows the tsunami wave profiles along transects following the canyon and ridge for the eight events mentioned earlier. The tsunami height profiles along the

canyon and ridge transects show the overall profile of the tsunami at different times, indicating the transformation of the tsunami profile with time. Figure 9 shows the tsunami wave heights at two locations closest to the coast (landfall point), viz. at the end of the canyon transect (point C2 in Figure 2) and another along the ridge transect (point R2 in Figure 2). A maximum tsunami height of about 2.3 m is observed at point C2 along the canyon transect, whereas at the landfall point along the ridge transect the maximum tsunami height is 4.5 m. Figure 10 presents the maximum tsunami wave height magnitude over the model domain for the first two waves. The tsunami amplitudes along the coast off the ridge are observed to be greater than the maximum values along the coast in line with the canyon.

Table 2 provides the measured tsunami run-up at the coast, model-derived maximum tsunami heights at 10 m as well as maximum velocities for seven locations (L1–L7; Figure 2), of which five are in close vicinity of the canyons and ridges. Maximum tsunami energy density ($E = 0.125\rho gH^2$) was estimated at 10 m depth contour for these locations and compared with the tsunami run-up observed on the coast from post-tsunami surveys carried out in the region (Figure 11). The tsunami energy and run-up height showed linear correlation.

Tsunami-induced currents

The tsunami-induced depth averaged flow velocity (current speed) vectors over the model domain at different times are shown in Figure 7, where the spatial variation of velocity magnitudes in relation with the tsunami crest and trough can be related. Prior to landfall of the tsunami on the coast along the canyon axis, convergence of flow velocity vectors along the ridge and divergence of flow vectors along the canyon axis were observed (Figure 7 *b* and *c*). The flow velocities were of the order of 0.1–0.55 m/s close to the coast whereas at 10 m water depth the flow velocities were of the order of 0.9–1.9 m/s. Figure 12 presents the tsunami-induced depth-averaged flow velocities at the eight snapshots as indicated in earlier sections along the canyon axis and ridge axis. Significant current speeds of the order of 1–1.25 m/s were observed along the canyon axis, whereas a maximum of about 0.5 m/s flow velocity was observed along the ridge transect. The flow velocity observed during the tsunami forward propagation was slightly lower than when the reflected tsunami wave propagates back into the ocean.

Discussion

Tsunami propagation

Figures 7 and 8 show the initial tsunami wavefront propagating from deep water to the continental shelf. The first

tsunami wavelength while the coast experiences the arrival of tsunami along the canyon axis about 3.20 h or 142 min from tsunami generation, was about 24 km with the tsunami height being 1.16 m at 7.8 km from the coast. At that moment the first tsunami wavelength along the ridge transect was 24 km (same as along the canyon) with a 1.9 m tsunami height located 14 km away from the coast. A snapshot of the tsunami profile during this time is not included. Till the initial tsunami front with amplitude 0.1 m reached the foot of the canyon and ridge, located about 45 km from coast, there was no change in the tsunami wavefront. The influence of first tsunami wave was felt at the foot of the ridge and canyon at about 2.57 h or 119 min from tsunami generation. As the tsunami traversed the canyon faster than along the ridge, the wavefront was affected by diffraction and refraction process and then divided into different parts. These different parts of the tsunami waves travel perpendicular to both the sides of the canyon as well as propagating along the canyon, thereby travelling at different wave

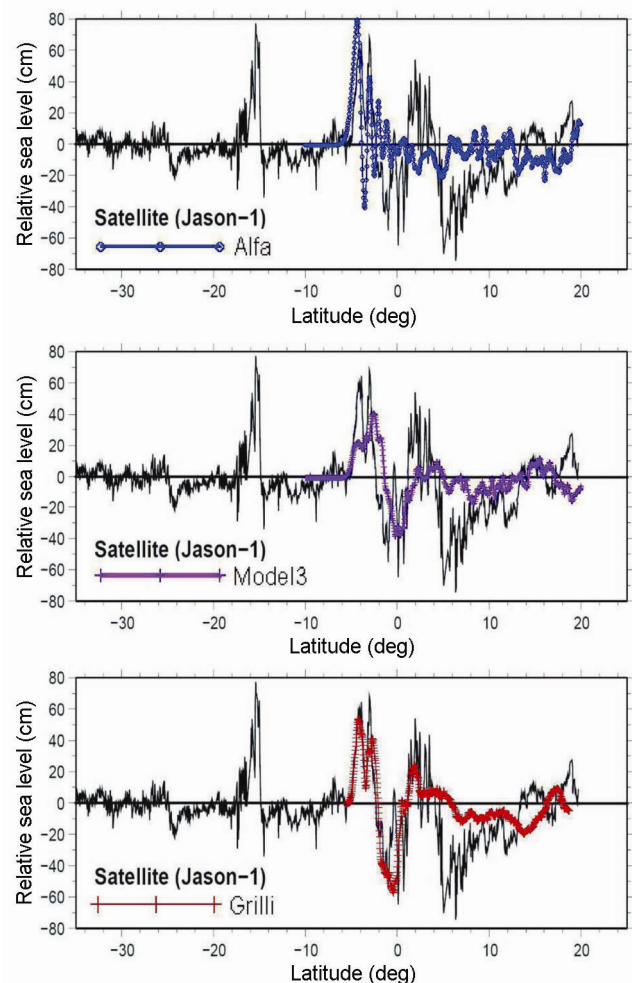


Figure 6. Comparison of MIKE21 model-derived tsunami surface elevation with satellite-derived data along Jason-1 satellite track using the tsunami source given by various initial tsunami source models.

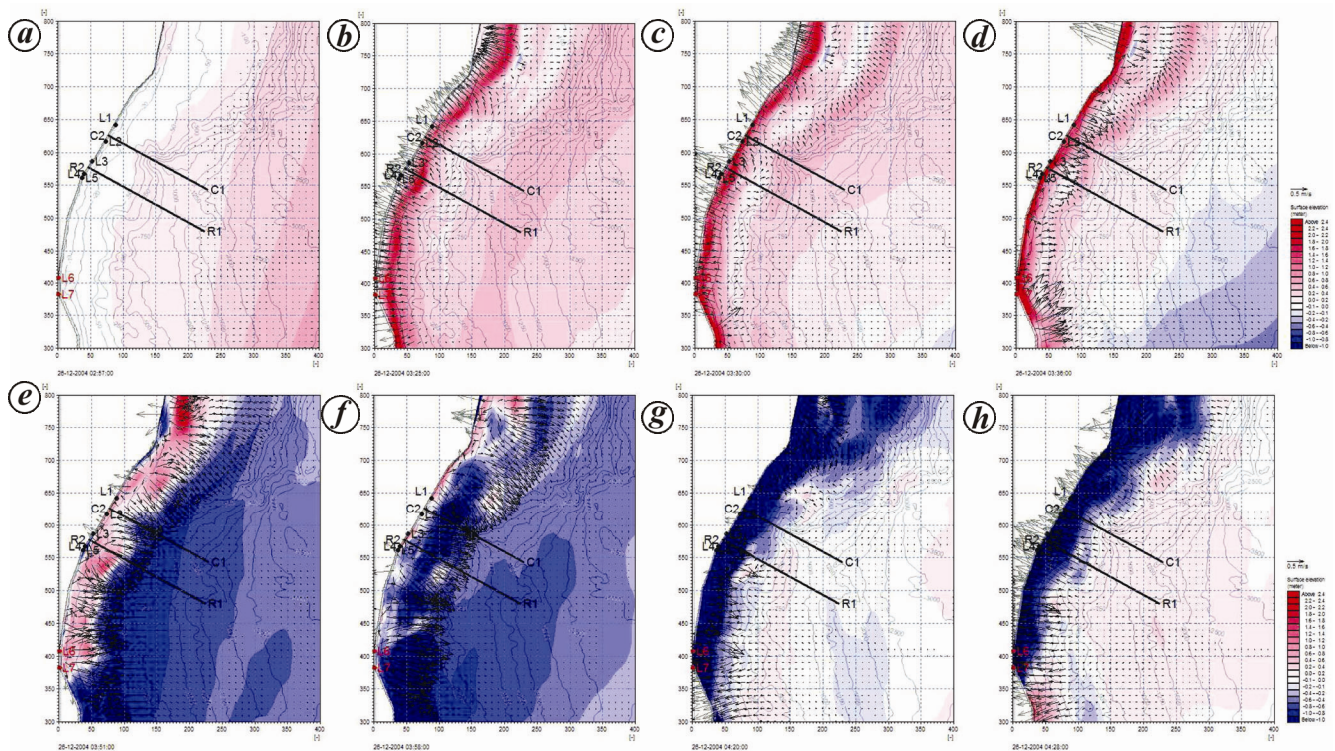


Figure 7. Plot showing tsunami height contours and flow velocity vectors at (a) 02 : 57 h; (b) 03 : 25 h; (c) 03 : 30 h; (d) 03 : 36 h; (e) 03 : 51 h (f) 03 : 58 h; (g) 04 : 20 h and (h) 04 : 28 h. Axes of the plots are grid numbers with each grid corresponding to 300 m square grid.

speeds as the water depths inside the canyon and along the canyon sides are different and transferring wave energy in the form of transmission–refraction process¹⁸.

As the tsunami wave traverses the canyon, at 3.25 h, about 147 min from the tsunami generation, the initial tsunami wave had its crest between the canyon head and the coast with an amplitude of 1.2 m about 3.6 km from the coast. At that instant the tsunami along the ridge had a wavelength of 21 km and tsunami amplitude of 2 m. From the coast the tsunami front can be seen coming closer along the canyon axis than along the ridge axis (Figure 7 b). Furthermore, it can be seen that wave amplitude within the canyon is lower than that along the ridge (Figure 8 b). As the initial tsunami wave crest with its maximum amplitude has its landfall at about 3.30 h (152 min from tsunami generation), the half wavelength is about 12 km with the amplitude being 2.3 m (Figure 8 c). After 6 min, the initial tsunami wave had its landfall with the tsunami amplitude being 4.5 m and the half wavelength being 11.4 km.

The crest of the tsunami second wave, although with lesser magnitude both along the canyon axis as well as along the ridge axis, had its landfall about 25 min from that of the initial crest (Figure 8 e and f). The drawdown or retreat of the tsunami was seen soon after the landfall of the second crest and the wave trough had its lowest elevation at about 4.20 h (about 202 min after the tsunami generation) for the wave along canyon axis and at about 4.28 h along the ridge axis (Figure 8 g and h). The differ-

ence between the landfall of wave crest/trough along the canyon axis and ridge axis was about 6–8 min for the canyon considered in this study.

The tsunami wave that travelled across the ridge before reaching the coast was observed to be more steep compared to that which travelled along the canyon. Also, the waves were observed to have a bore shape before becoming steep attaining solitary wave shape along and further surging ahead the coast. It can be seen from Figure 7 a that the wave crests propagate fairly parallel in deeper waters; the effect of the canyons is clearly seen in the first instance when the wave encounters the canyon or ridge toe. It is observed that the first wave reaches the coast earlier at locations along the canyon compared to surrounding locations due to the relatively faster propagation speeds along the canyon. Due to the deeper waters along the canyon, the tsunami propagates at relatively greater speed into the canyon whereas it propagates at relatively slow speed while it ‘climbs’ the slope of the ridge; the lower speeds of tsunami propagation being due to the shallow water encountered by it. As the shallow water wave speed is proportional to water depth, the tsunami velocity is lower along the ridge. The refraction and shoaling of tsunami-waves along ridge-slopes aid in concentrated convergent and divergent regions in the vicinity of the canyons and ridges. The tsunami front along the canyon propagates faster to the canyon head, but also diverges and propagates along the canyon slopes thereby diffusing its energy in transverse directions. The tsunami

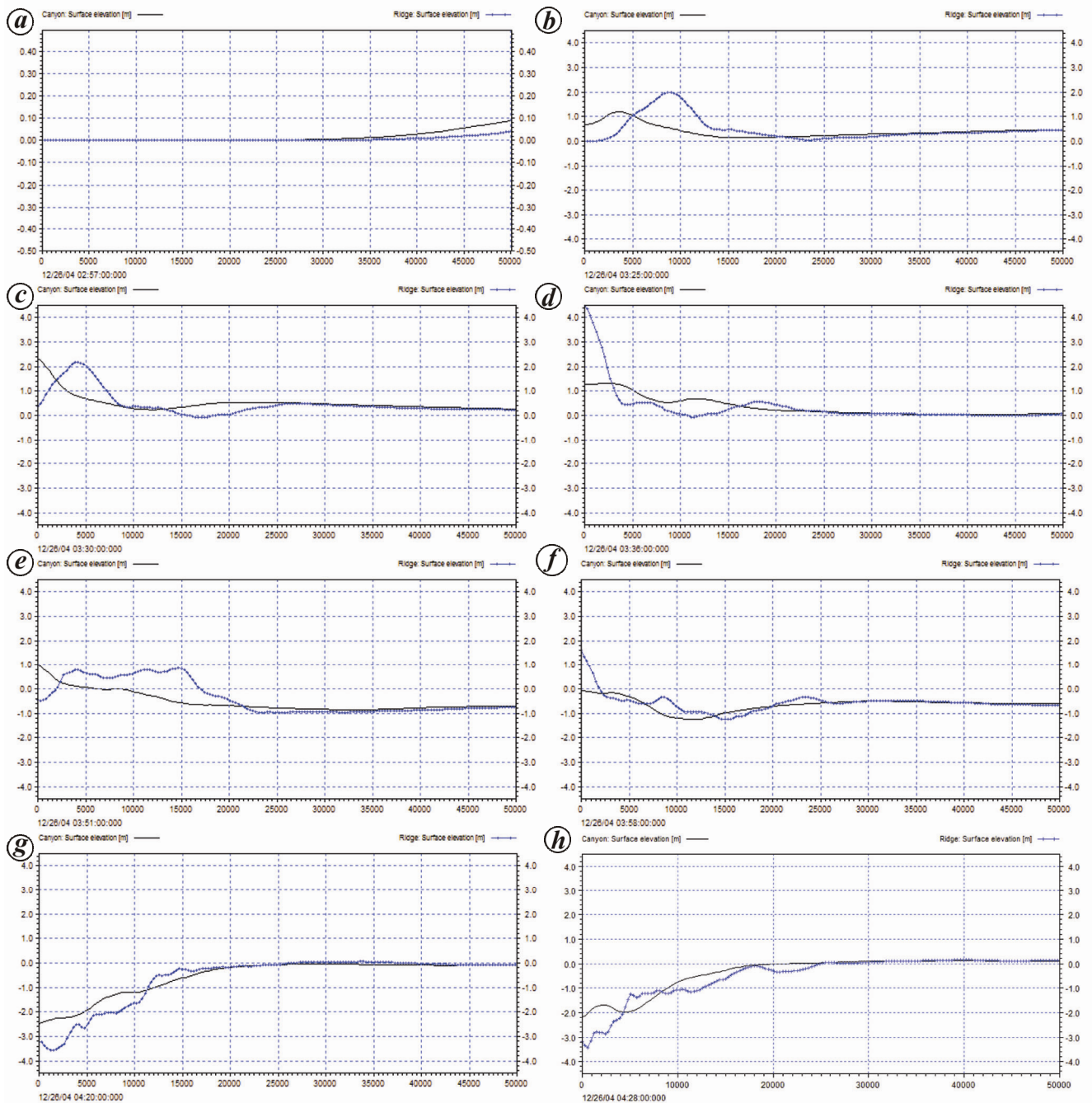


Figure 8. Plot showing tsunami height variation along the Pondicherry canyon (solid line; C1–C2) and Ridge (line with symbols; R1–R2) transects at (a) 02 : 57 h; (b) 03 : 25 h; (c) 03 : 30 h; (d) 03 : 36 h; (e) 03 : 51 h; (f) 03 : 58 h; (g) 04 : 20 h and (h) 04 : 28 h. The x-axis of the plot is distance (m) and the y-axis is surface elevation (m).

front propagation observed in this modelling study is similar to those carried out in the literature^{16,18,19}, wherein the processes of refraction, diffraction, shoaling, reflection and dissipation of tsunami waves are observed. The tsunami wave along the ridge is observed to be steeper than the tsunami profile along the canyon transect. Moreover, the drawdown during tsunami retreat is greater along the ridge transect compared to the canyon transect. The maximum tsunami heights obtained from the time of tsunami

impact on the coast till the first two waves reach the coast show that regions in line with the ridges have concentrated maximum heights and corresponding higher run-up heights, whereas locations along the canyon transect have comparatively lower tsunami heights and relatively lower run-up heights. These observations from the model results as well as from the field observations are consistent with those reported in the literature¹⁸. The reason for abrupt changes in the run-up heights along the southeast

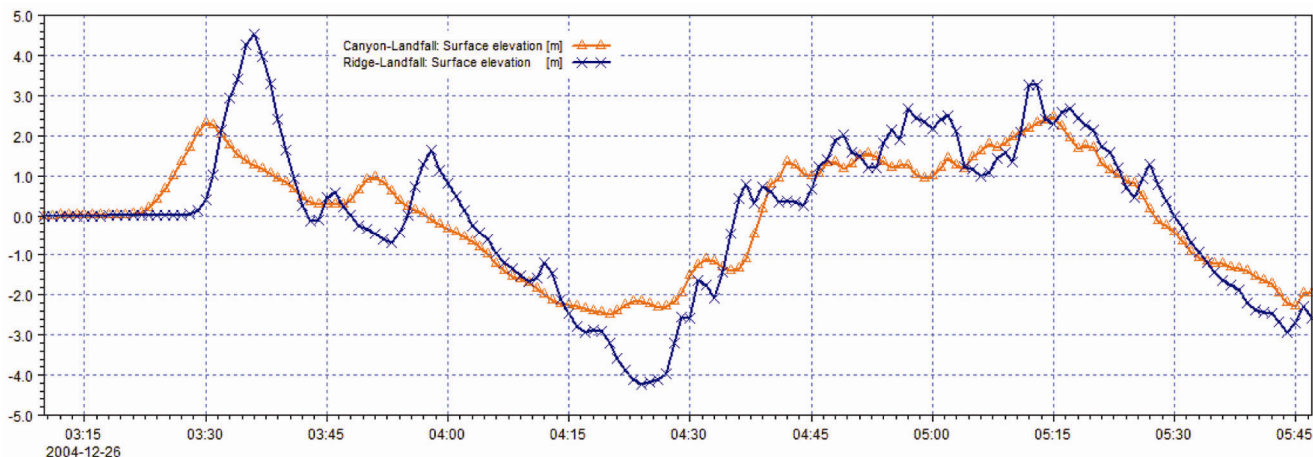


Figure 9. Plot showing tsunami height variation at the landfall points at end of canyon transect (line with triangles; C2) and at landfall point along ridge transect (line with crosses; R2). The x-axis of the plot is time (h : min) and y-axis is surface elevation (m).

Table 2. Locations considered along the study region with the run-up height observations and model results of tsunami heights and velocities using tsunami source from Grill *et al.*⁴⁰

Station no.	Station	Position		Run-up height* (m)	Maximum tsunami amplitude at 10 m depth (m)	Maximum tsunami velocity at 10 m depth (m/s)	Maximum tsunami amplitude at coast (m)
		Latitude (°N)	Longitude (°E)				
L1	Kottai Kadu Kuppam	12°14'42.00"	79°58'59.04"	2.498	1.34	1.05	2.52
L2	Ekkiar Kuppam	12°10'49.00"	79°57'37.03"	4.525	1.88	0.89	2.39
L3	Nochi Kuppam	12°05'08.46"	79°53'55.01"	3.727	1.97	1.51	3.7
L4	Periyakalpet (North)	12°02'03.18"	79°52'17.07"	5.362	2.4	1.86	4.6
L5	Periyakalpet (South)	12°01'00.00"	12°51'00.00"	5.886	2.29	1.92	4.3
L6	Kurinjipadi	11°36'45.03"	79°45'34.08"	3.722	1.75	1.38	3.26
L7	Velangirayan	11°31'58.8"	79°45'00.00"	3.663	1.87	1.60	3.26

*Run-up heights taken from Ilangoan *et al.*²⁷.

coast of India, wherein the run-up heights were higher at a location by 50% is clearly seen from this study. The locations where higher run-up heights observed in the field are in line with the ridge (locations L3–L5), whereas at locations L1 and L2 which are in line with the canyon showed relatively lower run-up heights (Figure 10). Thus the influence of canyon on tsunami heights and run-up is significant southeast coast of India. Apart from the regions adjacent to canyon-ridge system, concentration of maximum tsunami heights can also be seen at other locations both towards north and south of Pondicherry Canyon, which could be attributed to a comparatively wider continental shelf width than near the canyons⁵⁰.

The pattern of variation of the observed run-up heights is consistent with the variation in the modelled tsunami heights along the study region, with maximum run-up occurring along the ridge between Cuddalore and Pondicherry canyons. A linear trend between the run-up height and tsunami energy density estimated at 10 m water depth is observed at these locations. The run-up heights were observed to be about 0.1% ($R^2 > 0.9$) of the wave energy

density at 10 m water depth for the open coast (Figure 11). However, this linear relationship needs to be further studied considering other parameters (e.g. shelf width, tsunami period, etc.).

Tsunami-induced currents

The current speed along the canyon axis gradually increased and peaked to 1 m/s at around 3.26 h when the crest of the initial wave had its landfall on the coast, with the peak currents being experienced at about 2.7 km from the coast (Figure 12), whereas during this time the peak current speed along the ridge axis was 1.2 m/s. However, during the initial wave crest landfall at 3.30 h, the peak current speed rapidly reduced by more than 70% within 4 min resulting due to rapid transition in the flow velocities. At this time the current speed along the ridge axis peaked to 1.5 m/s. However, the current speed along the ridge axis peaked to 1.7 m/s at 3.33 h, i.e. about 3 min before the initial wave crest had its landfall. The current speed rapidly reduced from 1.7 to 0.4 m/s in about 4 min.

Such rapid changes in the current speeds in the region would cause severe turbulence affecting the seabed, thereby bringing the sediments into suspension. This rapid change in currents corroborates the eyewitness accounts indicating turbulent and muddy waters in the nearshore regions. The second tsunami wave-induced current speeds were of similar order of magnitude (~ 1 m/s) for both the regions along the canyon axis as well as ridge axis. The current speeds during initial wave trough or drawdown were similar to the peak speeds observed during tsunami advancement.

Flow velocities induced by the tsunami, as seen in the present numerical model, were observed to be in the maximum magnitude range 1–1.25 m/s along the Pondicherry Canyon. The current speed was greater at 10 m water depth compared to the speed closer to the coast. The flow velocities in the canyon were greater than the flow velocities along the ridge, which is consistent with the observations made in other studies^{18–20}. Focusing of velocity vectors on the shelf region of the ridge and divergence of velocity vectors at the canyon head can be clearly observed in this study. Steepening of tsunami wave causes convergence of flow velocity vectors on both sides of the canyon and divergence along the canyon head.

Canyon impact on tsunami vis-à-vis other literature results

Iglesias *et al.*¹⁹ analysed the results of tsunami propagation over synthetic submarine canyons and concluded that there is a strong variation of tsunami arrival times and tsunami amplitudes on the coastline for tsunami propagation over submarine canyon, with changing maximum height location and alongshore extension. Their study indicated that the presence of a submarine canyon not only reduces the arrival time at the shore but also prevents tsunami amplification just over the canyon axis, leading to a decreased tsunami height along the stretch of the coast shoreward of the canyon head. They also observed increased tsunami height on both sides of the canyon head, generating two stretches of the coast with increased tsunami run-up. Similar to the results of Iglesias *et al.*¹⁹, the present study also shows reduced tsunami amplitude along the canyon axis resulting in reduced tsunami run-up and increased tsunami amplitude along the coast facing the ridge.

Although Grilli *et al.*⁴⁰ and Ioualalen *et al.*²⁰ used the same initial tsunami surface elevation which is employed in the present study and simulated tsunami propagation in the Bay of Bengal, both these studies did not report tsunami propagation and impacts of canyons related to the Pondicherry Canyon or the southeast coast of India. While Grilli *et al.*⁴⁰ focused on the Thailand coast, Ioualalen *et al.*²⁰ focused on the Bangladesh coast, especially on the propagation through the submarine canyon off

Bangladesh coast. Ioualalen *et al.*²⁰ could not validate their results due to lack of measurements and could not attribute the increased tsunami impact along the canyon axis. However, through their study it is made clear that

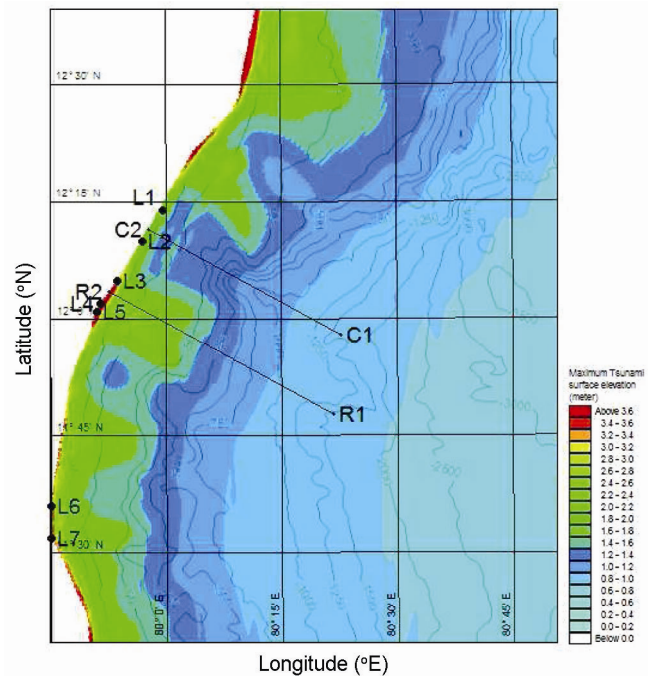


Figure 10. Maximum tsunami heights in the study region considering the first and second waves. Locations for comparing run-up heights with tsunami energy are shown as L1–L7.

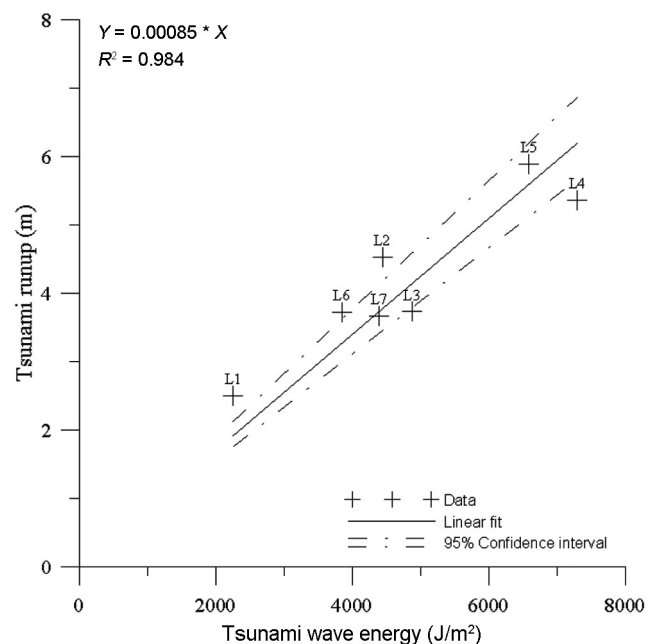


Figure 11. Plot showing measured run-up height versus wave energy density at 10 m contour. The dashed lines represent 95% confidence limits. L1–L7 represent locations mentioned in Table 2.

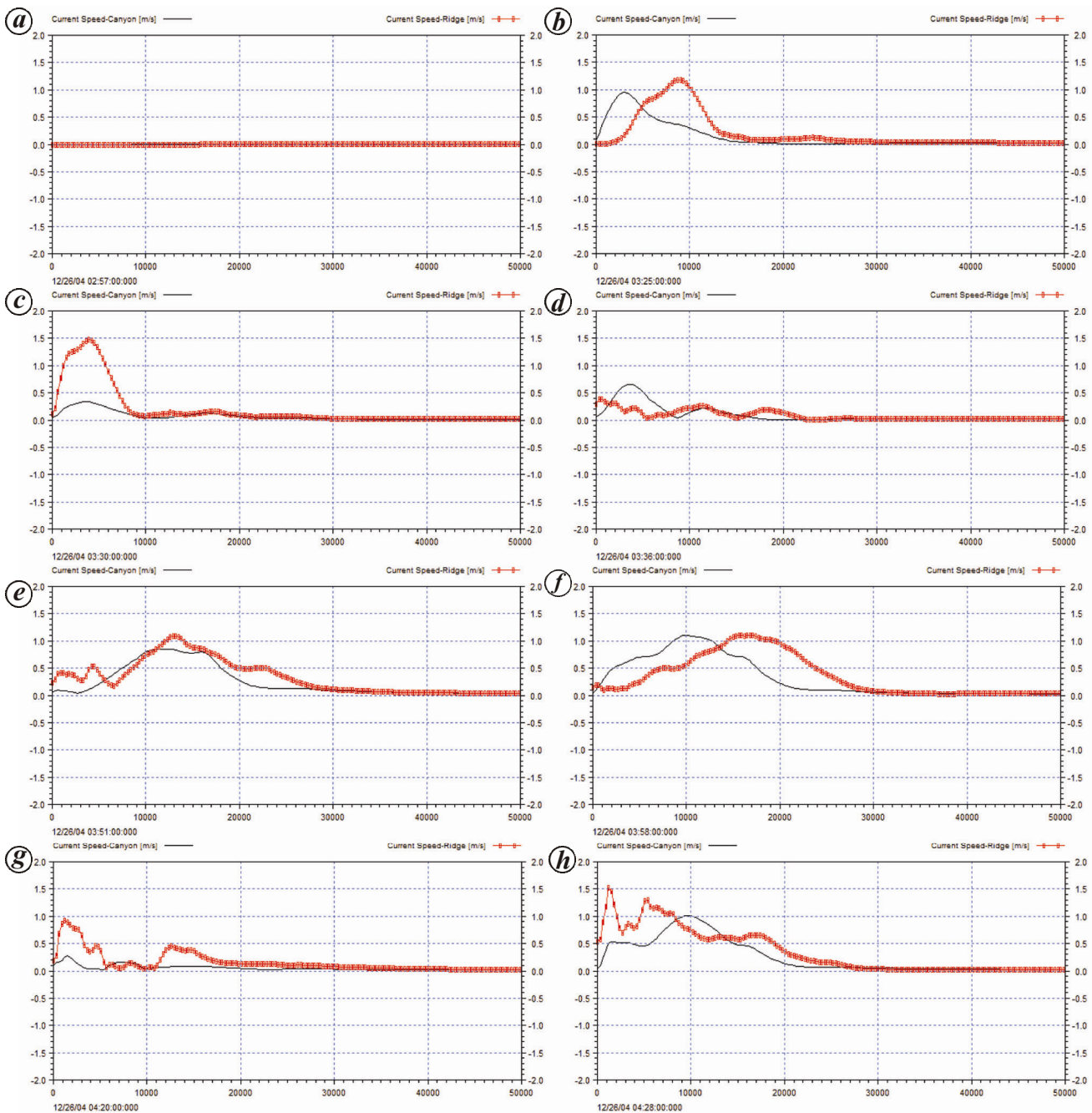


Figure 12. Plot showing tsunami-induced current speed variation along the Pondicherry canyon (solid line) and ridge (line with symbols) transects at (a) 02 : 57 h; (b) 03 : 25 h; (c) 03 : 30 h; (d) 03 : 36 h; (e) 03 : 51 h; (f); 03 : 58 h; (g) 04 : 20 h and (h) 04 : 28 h. The x-axis of the plot is distance (m) and the y-axis is current speed (m/s).

the effects of nonlinearity, bottom friction or dispersion are not significant for tsunami propagation along submarine canyons. The results of the present study are largely in tune with general properties of tsunami propagation along ridges. The results corroborate with the results of Ioualalen *et al.*²⁰, wherein increased tsunami impact away from the canyon axis was reported in terms of high wave activity east of the canyon which runs in NE direction. The maximum tsunami amplitude along the coast abut-

ting the flanks of canyon or along the ridge was observed to be about 4.52 m, whereas along the coast abutting the canyon axis the tsunami amplitude was observed to be 2.3 m. The amplification due to the presence of canyon was about two times, which was similar to the studies carried out by Roger and Hébert¹⁷ for the coast of Balearic Islands, wherein a tsunami amplification of about two times was estimated on both sides of the canyon.

There are no physical measurements of current speeds available in the canyon or ridge region along the southeast coast of India during the tsunami to validate the model results. The magnitude of the depth-averaged current speeds was of the order of 0.5–2 m/s over the canyon; this requires further validation through application of a validated 3D model with water depth resolved in the vertical.

Conclusion

Tsunami propagation modelling has been carried out to study the tsunami heights and flow velocities in the vicinity of submarine canyons off the southeast coast of India. Tsunami amplitudes and arrival times were validated with field observations to a higher accuracy. Considerable effects of tsunami focusing, tsunami amplification and flow velocity enhancement, around the submarine canyons and ridges are observed from the model studies. Focusing occurs on the ridges, leading to a complex variation in tsunami heights and currents in the nearshore (10 m contour). Maximum tsunami heights over the ridges are approximately twice those in the canyons. The pattern of modelled tsunami height and observed run-up is similar to maximum height along the ridge transects and minimum heights along canyon transects. The same pattern is observed in the run-up limits observed in the field, with two of the largest run-up heights along the abutting the ridges and two of the lowest run-up heights along the coast abutting the canyons. Observed run-up height was proportional to the tsunami wave energy density at the 10 m contour with a R^2 more than 0.98, showing that wave energy at the 10 m contour is proportional to the tsunami run-up heights for open coasts, irrespective of the presence of submarine canyons. The results of the present study are consistent with those regarding influence of canyon on tsunami amplitudes. Tsunami-induced current speeds showed higher values along the ridge axis compared to those along the canyon axis. The current speed during the drawdown is observed to be slightly higher than that during tsunami advancement.

1. Geist, E. and Yoshioka, S., Source parameters controlling the generation and propagation of potential local tsunamis along the cascadia margin. *Nat. Hazards*, 1996, **13**(2), 151–177.
2. Titov, V. *et al.*, The global reach of the 26 December 2004 Sumatra Tsunami. *Science*, 2005, **309**(5743), 2045–2048.
3. Shanmugam, G., Slides, slumps, debris flows and turbidity currents. In *Encyclopedia of Ocean Sciences* (eds John, H. S. *et al.*), Academic Press: Oxford, 2009, pp. 447–467.
4. Jaya Kumar, S. *et al.*, Run-up and inundation limits along southeast coast of India during the 26 December 2004 Indian Ocean tsunami. *Curr. Sci.*, 2005, **88**(11), 1741–1743.
5. Jaya Kumar, S. *et al.*, Tsunami height estimation in nearshore waters off Tamil Nadu coast using MIKE21 hydrodynamic model for the December 2004 Indian Ocean tsunami. In 15th Congress of Asia and Pacific Division of the International Association for Hydraulic Research and International Symposium on ‘Maritime Hydraulics’, IIT Madras Chennai, India, 2006.
6. Murthy, K. S. R. *et al.*, Factors guiding tsunami surge at the Nagapattinam–Cuddalore shelf, Tamil Nadu, east coast of India. *Curr. Sci.*, 2006, **90**(11), 1535–1538.
7. Bhaskaran, P. K. *et al.*, *Tsunami Travel Time Atlas for the Indian Ocean*, Indian Institute of Technology, Kharagpur, 2005, p. 279.
8. Bhaskaran, P. K. and Pandey, P. C., Tsunami early warning system: an Indian Ocean perspective. *Nat. Anthropogenic Disasters*, 2010, 100–125.
9. Bhaskaran, P. K. *et al.*, Tsunami travel time computation and skill assessment for the 26 December 2004 event in the Indian Ocean. *Coast. Eng. J.*, 2006, **48**(2), 147–166.
10. Barman, R. *et al.*, Tsunami travel time prediction using neural networks. *Geophys. Res. Lett.*, 2006, **33**, L16612.
11. Bhaskaran, P. K. *et al.*, Tsunami early warning system – an Indian Ocean perspective. *J. Earthq. Tsunami*, 2008, **2**(3), 197–226.
12. Sudha Rani, N. N. V. *et al.*, Coastal vulnerability assessment studies over India: a review. *Nat. Hazards*, 2015, **77**, 405–428.
13. Seelam, J. K. and Baldock, T. E., Role of submarine canyon on tsunami amplification on south east coast of India. In International Conference of Asia Oceania Geosciences Society (AOGS 2009), Singapore, 2009.
14. Divyalakshmi, K. S. *et al.*, Modification of tsunami wave by submarine canyon: case study of multiple canyons at south east coast of India. *Mar. Geodesy*, 2011, **34**(1), 2–15.
15. Seelam, J. K. and Baldock, T. E., Tsunami induced shear stresses along submarine canyon off southeast coast of India. In Sixth International Conference of Asia and Pacific Coasts (APAC 2011), Hong Kong, 2011.
16. Jindasa, S. U. P., Evaluation of 26 December 2004 tsunami wave hazardness with coastal bathymetry and geomorphology. A case study in Sri Lanka. *Dis. Adv.*, 2008, **1**(4), 27–31.
17. Roger, J. and Hébert, H., The 1856 Djijelli (Algeria) earthquake and tsunami: source parameters and implications for tsunami hazard in the Balearic Islands. *Nat. Hazards Earth Syst. Sci.*, 2008, **8**, 721–731.
18. Aránguiz, R. and Shibayama, T., The effect of submarine canyon on tsunami propagation: a case study of the Biobio Canyon, Chile. *Coast. Eng. J.*, 2013, **55**, 1350016.
19. Iglesias, O. *et al.*, Effects of coastal submarine canyons on tsunami propagation and impact. *Mar. Geol.*, 2014, **350**, 39–51.
20. Ioualalen, M. *et al.*, On the weak impact of the 26 December Indian Ocean tsunami on the Bangladesh coast. *Nat. Hazards Earth Syst. Sci.*, 2007, **7**, 141–147.
21. Baldock, T. E. *et al.*, Modelling tsunami inundation on coastlines with characteristic form. In 16th Australasian Fluid Mechanics Conference (AFMC), Queensland, Australia, 2007, pp. 939–942.
22. Didenkulova, I. and Pelinovsky, E., Runup of tsunami waves in U-shaped bays. *Pure Appl. Geophys.*, 2011, **168**, 1239–1249.
23. Zahibo, N. *et al.*, Tsunami wave run-up on coasts of narrow bays. *Int. J. Fluid Mech. Res.*, 2006, **33**, 106–118.
24. Directorate of town and country planning, GOTN, Coastal zone management plan for Tamil Nadu, Government of Tamil Nadu, Chennai, June 1996.
25. Varadachari, V. V. R. *et al.*, Submarine canyons off the Coromandel coast. *Bull. Natl. Inst. Sci. India*, 1968, **38**, 457–462.
26. Shetty, M. G. A. P., Submarine canyons off Madras coast. *Curr. Sci.*, 1964, **33**(20), 685.
27. Ilangovan, D. *et al.*, Inundation, run-up heights, cross-section profiles and littoral environment along the Tamil Nadu coast after 26 December 2004 Tsunami, National Institute of Oceanography, Goa, 2005.
28. Jain, S. K. *et al.*, Effects of M9 Sumatra earthquake and tsunami of 26 December 2004. *Curr. Sci.*, 2005, **88**(3), 357–359.
29. Ramanamurthy, M. V. *et al.*, Inundation of sea water in Andaman and Nicobar Islands and parts of Tamil Nadu coast during 2004 Sumatra tsunami. *Curr. Sci.*, 2005, **88**(11), 1736–1740.

RESEARCH ARTICLES

30. Chadha, R. K. *et al.*, The tsunami of the great Sumatra earthquake of *M* 9.0 on 26 December, 2004 – impact on the east coast of India. *Curr. Sci.*, 2005, **88**, 1297–1301.
31. Kurian, N. P. *et al.*, Inundation characteristics and geomorphological impacts of December 2004 tsunami on Kerala coast. *Curr. Sci.*, 2006, **90**, 240–249.
32. Jaya Kumar, S. *et al.*, Post-tsunami changes in the littoral environment along the southeast coast of India. *J. Environ. Manage.*, 2008, **89**(1), 35–44.
33. Pari, Y. *et al.*, Morphological changes at Vellar estuary, India – impact of the December 2004 tsunami. *J. Environ. Manage.*, 2008, **89**(1), 45–57.
34. Sundar, V. *et al.*, Runup and inundation along the Indian Peninsula, including the Andaman Islands, due to great Indian Ocean tsunami. *J. Waterway Port Coastal Ocean Eng.*, 2007, **133**, 401–413.
35. UNESCO, Post-Tsunami Survey Manual, Intergovernmental Oceanographic Commission Manual No. 37, edn. UNESCO IOC/ITIC, 2002.
36. Bhattacharya, G. C. *et al.*, Observations of post tsunami reconnaissance investigations along eastern coastal tract of India following the devastating tsunami of 26 December 2004, CSIR-National Institute of Oceanography: Dona Paula, Goa, India, 2005, p. 109.
37. Seelam, J. K. and Volvaiker, S. S., Tsunami heights off southeast Indian coast from run-up measurements. In International Conference of Asia Oceania Geosciences Society (AOGS 2009), Singapore, 2009.
38. DHI, Mike21 flow model – hydrodynamic module – scientific documentation, DHI, Denmark, 2011 (cited 2011 25/05/2011); <http://www.mikebydhi.com/Products/CoastAndSea/MIKE21/Hydro-dynamics.aspx>
39. Neetu, S. *et al.*, Comment on The Great Sumatra–Andaman earthquake of 26 December 2004. *Science*, 2005, **310**(5753), 1431.
40. Grilli, S. T. *et al.*, Source constraints and model simulation of the 26 December 2004, Indian Ocean tsunami. *J. Waterway, Port, Coastal Ocean Eng.*, 2007, **133**(6), 414–428.
41. Pietrzak, J. *et al.*, Defining the source region of the Indian Ocean tsunami from GPS, altimeters, tide gauges and tsunami models. *Earth Planet. Sci. Lett.*, 2007, **261**(1–2), 49–64.
42. Smit, P. B. *et al.*, Assessment of non-hydrostatic wave-flow model SWASH for directionally spread waves propagating through a barred basin. In Fifth International Conference on Advanced Computational Methods in Engineering (ACOMEN 2011), Liège, Belgium, 2011, pp. 1–10.
43. Vigny, C. *et al.*, Insight into the 2004 Sumatra–Andaman earthquake from GPS measurements in Southeast Asia. *Nature*, 2005, **436**(7048), 201–206.
44. Song, Y. T. *et al.*, The 26 December 2004 tsunami source estimated from satellite radar altimetry and seismic waves. *Geophys. Res. Lett.*, 2005, **32**(20), 20601.
45. Pedersen, N. H. *et al.*, Modelling of the Asian tsunami off the coast of northern Sumatra, in DHI Users Conference, Malaysia, 2005.
46. Okada, Y., Surface deformation due to shear and tensile faults in a half-space. *Bull. Seismol. Soc. Am.*, 1985, **75**(41), 1135–1154.
47. Wei, G. and Kirby, J. T., A time-dependent numerical code for extended Boussinesq equations. *J. Waterway, Port, Coastal Ocean Eng.*, 1995, **121**, 251–261.
48. Ritchmeyer, R. D. and Morton, K. W., *Difference Methods for Initial Value Problems*. Interscience, New York, 1967, 2nd edn.
49. Nagarajan, B. *et al.*, The great tsunami of 26 December 2004: a description based on tide gauge data from Indian subcontinent and surrounding areas. *Earth Planets Space*, 2006, **58**, 211–215.
50. Goring, D. G., *Tsunamis – the propagation of long waves onto a shelf*, Caltech, CA, USA, 1978.

ACKNOWLEDGEMENTS. We thank our respective organizations for infrastructure facilities and support and the anonymous reviewers for their comments that helped improve the manuscript.

Received 22 January 2015; revised accepted 15 July 2016

doi: 10.18520/cs/v111/i12/1990-2004
